nature nanotechnology

LETTERS

PUBLISHED ONLINE: 4 AUGUST 2013 | DOI: 10.1038/NNANO.2013.146

Luminescence upconversion in colloidal double quantum dots

Zvicka Deutsch†, Lior Neeman† and Dan Oron*

Luminescence upconversion nanocrystals capable of converting two low-energy photons into a single photon at a higher energy are sought-after for a variety of applications, including bioimaging[1,2] and photovoltaic light harvesting[3]. Currently available systems, based on rare-earth-doped dielectrics[4,5], are limited in both tunability and absorption cross-section. Here we present colloidal double quantum dots as an alternative nanocrystalline upconversion system, combining the stability of an inorganic crystalline structure with the spectral tunability afforded by quantum confinement. By tailoring its composition and morphology, we form a semiconducting nanostructure in which excited electrons are delocalized over the entire structure, but a double potential well is formed for holes. Upconversion occurs by excitation of an electron in the lower energy transition, followed by intraband absorption of the hole, allowing it to cross the barrier to a higher energy state. An overall conversion efficiency of 0.1% per double excitation event is achieved.

The ability to upconvert two low-energy photons into a single higher-energy photon is of significant importance in many fields. In biomedical imaging, upconversion enables spatially resolved imaging in a scattering specimen. In photovoltaic devices, upconversion could be used as a potential method for surpassing the Shockley–Queisser efficiency limit[6] by utilization of photons with energies below the bandgap of the absorber. Generally, however, efficient room-temperature upconversion is very difficult to achieve, and typically requires significant electromagnetic field intensities, such as those obtained by focusing coherent laser radiation. Indeed, coherent conversion processes, in particular second-harmonic or sum frequency generation, are commonly used to upconvert laser light. However, because decoherence processes are extremely rapid, upconversion at low illumination intensities is much more difficult to achieve. Efficient upconversion requires the existence of a long-lived metastable state, which can be further promoted to generate a higher energy emission. The prototypical system for achieving this makes use of rare-earth-doped glasses, in which a variety of such states are available. As it relies on atomic lines, rare-earth-based upconversion can also be realized in nanocrystals[7]. Despite recent progress using, for example, dopant blends[8] and hybrid organic–inorganic systems[9], this system suffers from low colour tunability and relatively low absorption cross-sections. Another alternative system for upconversion is triplet–triplet annihilation[10–13], whereby two molecules excited to a long-lived triplet state transfer their excitation to a higher-energy singlet state of another molecule. Although tunable by appropriate choice of the organic molecule, this system suffers from several drawbacks, including the limited availability of near-infrared fluorophores and photobleaching.

Here we propose and demonstrate a new system for luminescence upconversion in semiconductor nanocrystals, a field that has recently witnessed dramatic advancements in synthetic capabilities, enabling the manufacture of complex multicomponent systems[14–16]. It is based on a unique design comprising a compound semiconductor nanocrystal, which incorporates two quantum dots with different bandgaps separated by a tunnelling barrier. A schematic description of the structure, which we have recently shown[17] to function as a two-colour quantum emitter, is presented in Fig. 1a. Upconversion is expected to occur by the sequential absorption of two photons. In broad terms, the first excites an electron–hole pair via interband absorption in the lower-energy core, leaving a confined hole and a relatively delocalized electron. The second absorbed photon can lead, either directly or indirectly, to further excitation of the hole, enabling it to then cross the barrier layer. This, in turn, is followed by radiative recombination with the delocalized electron.

The two possible mechanisms by which upconversion could take place are schematically outlined in Fig. 1d,e. The first is direct intraband absorption of the second photon by the hole (Fig. 1d). The other is an Auger-mediated transition, whereby two excitons are initially formed in the core, and non-radiative Auger recombination of one electron–hole pair provides energy for ejection of the second hole (Fig. 1e)[18]. The latter mechanism is reminiscent of attempts to achieve upconversion in quantum-well-based devices[19–23]. In these, multiple excitations of a low-bandgap quantum well interact with one another via the Auger mechanism, leading to ejection of carriers from the quantum well to the host, and resulting in higher-energy luminescence (the effect is also known as an 'Auger fountain'). As we show below, the dominant mechanism in our nanocrystals is, unlike in the case of quantum wells, intraband absorption. Moreover, our quantum dots are operational at room temperature whereas quantum well upconversion is often limited to temperatures below that of liquid nitrogen.

To experimentally realize the system portrayed in Fig. 1a, we modified our previously reported[17] synthetic procedure to dramatically enhance emission quantum yields, reproducibility and particle uniformity. Tellurium-doped CdSe nanocrystals (diameter[24] of 4 nm) were used as seeds for over-growth of ~40 nm CdS nanorods[25,26]. At the tip of the nanorods, small amounts of Cd and Se were deposited to form a second CdSe dot, leading to the emergence of a second emission colour from the nanocrystals, as shown in Fig. 1c. The centroids of the two emissions in the final product are at 570 and 690 nm. The higher-energy emission colour can be controlled by tuning the size of the second CdSe dot. A transmission electron microscopy (TEM) image of the nanocrystals is shown in Fig. 1b. Exciting at 400 nm, the quantum yield of both emissions combined was measured to be ~42% (with a ratio of ~10:1 in favour of the lower-energy emission). Further details on synthesis and nanocrystal characterization can be found in Supplementary Section S1.

To examine the prospect of upconversion in this system we first illuminated a dilute solution of the nanocrystals in toluene with

Department of Physics of Complex Systems, Weizmann Institute of Science, Rehovot 76100, Israel, †These authors contributed equally to this work.
*e-mail: dan.oron@weizmann.ac.il

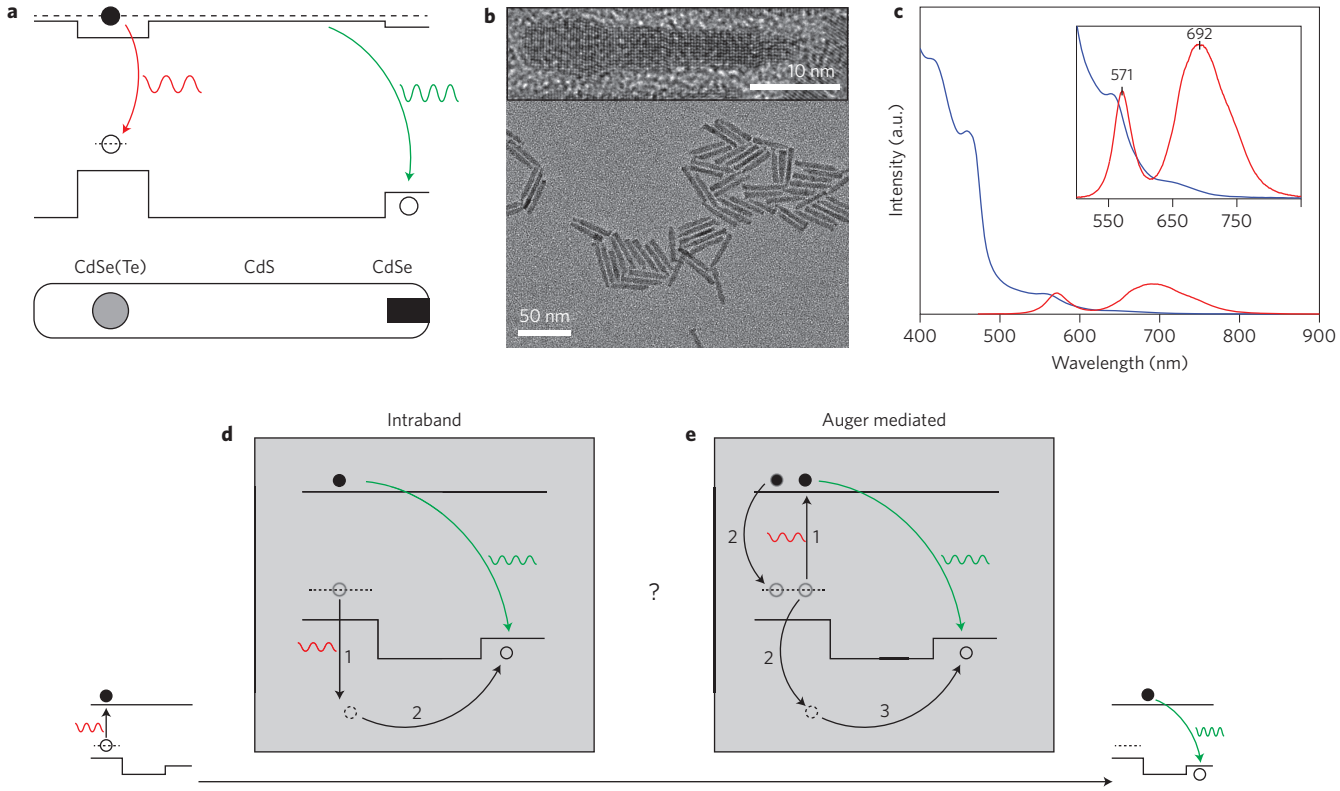

Figure 1 | Description of the upconversion nanocrystals. a, Schematic depiction of dual emitting quantum dot. The low-energy transition (red arrow) results from the hole localized in the doped core and the high-energy transition (green arrow) results from the second CdSe dot at the tip of the CdS barrier. **b**, TEM image of the nanocrystals. A magnified view of a single nanocrystal is presented at the top. **c**, Ensemble absorption (blue) and emission (red) spectra. The CdS absorption is visible around 460 nm. Inset: magnified view of the spectral region around the two emissions. **d**, Direct intraband hole absorption mechanism of upconversion: a hot hole formed due to intraband absorption (1) crosses above the barrier to the second dot (2). **e**, Auger-mediated upconversion: a second intraband absorption event (1) is followed by Auger recombination, leading to a formation of a hot hole (2), which then crosses above the barrier to the second dot (3).

5 ns, 680 nm pulses and measured the emission around 570 nm. The pulse duration is much shorter than the radiative lifetime of the lower energy emission (~100 ns). Thus, multiple excitations can occur within the same pulse, leading to upconversion. Indeed, the emission spectrum of the upconverted luminescence, plotted in Fig. 2a, closely follows the ensemble emission (the sharp rise at ~630 nm is due to directly excited emission from the core). As upconversion requires the successive absorption of two red photons, a quadratic dependence of the upconverted intensity with excitation pulse energy is expected at low excitation intensities. Upon saturation (that is, when the probability of absorption of at least one photon per particle within the pulse approaches unity), the dependence should turn linear[27]. As can be seen in Fig. 2b, this trend is indeed observed, with the roll-off occurring at an excitation density of ~0.4 mJ cm^{-2}. This value is somewhat lower than the saturation excitation density of the 680 nm emission, which is ~0.93 mJ cm^{-2}, as shown in Fig. 2c. This indicates that upconversion in our system is dominated by the intraband absorption mechanism depicted in Fig. 1d, rather than the Auger-mediated mechanism described in Fig. 1e. In the latter mechanism the roll-off would be expected to occur at a higher excitation density than the linear emission saturation of the 'red' dot (0.93 mJ cm^{-2}) due to the lower probability of a second interband excitation[24].

To substantiate our proposition that intraband absorption is playing a significant role, we performed a pump–probe experiment, where the 5 ns, 680 nm pump pulse is followed, 22 ns later, by a 5 ns near-infrared pulse at 1,064 nm, which cannot induce interband absorption in this system. Figure 3a shows that a weak upconversion signal due to the relatively weak 680 nm pump pulse is followed by a steep rise upon the arrival of the delayed 1,064 nm probe pulse. This clearly shows that intraband hole absorption is in play. Remarkably, as presented in Fig. 3b, a drop in the intensity of the red emission transient is revealed due to partial depletion by the probe pulse. The increase in upconverted emission intensity is linear in the probe pulse energy density (Fig. 3c), as expected. Moreover, when fixing the probe energy, while scanning the wavelength of the pump, the upconversion intensity is simply proportional to the ensemble absorption cross-section (Fig. 3d), further evidence of a simple, two-step upconversion process.

Once a hot hole is excited in the core, the overall efficiency of the upconversion process is determined by the multiplication of two probabilities—the probability of a hot hole crossing the barrier and the radiative quantum yield of the 570 nm emission. To estimate the former, we measure the saturation intensity of the 570 nm luminescence upon saturated excitation at 500 nm, which serves as a reference to the quantum dot concentration. We then measure, using the same set-up and upon excitation at 680 nm with 0.93 mJ cm^{-2} per pulse, that the upconverted emission is ~570 times weaker. By considering the statistics of photon absorption (Supplementary Section S3), the number of hot holes formed can be estimated. The probability of a hot hole crossing the barrier is calculated to be ~1%. The 570 nm emission quantum yield can be estimated from the ensemble absolute quantum yield data to be at least 10% (Supplementary Section S3). Neglecting absorption events not leading to the excitation of a hot hole, the maximum upconversion efficiency under saturated excitation (often termed elsewhere as the 'upconversion quantum yield') can thus be estimated to ~0.1%. As discussed above, interband

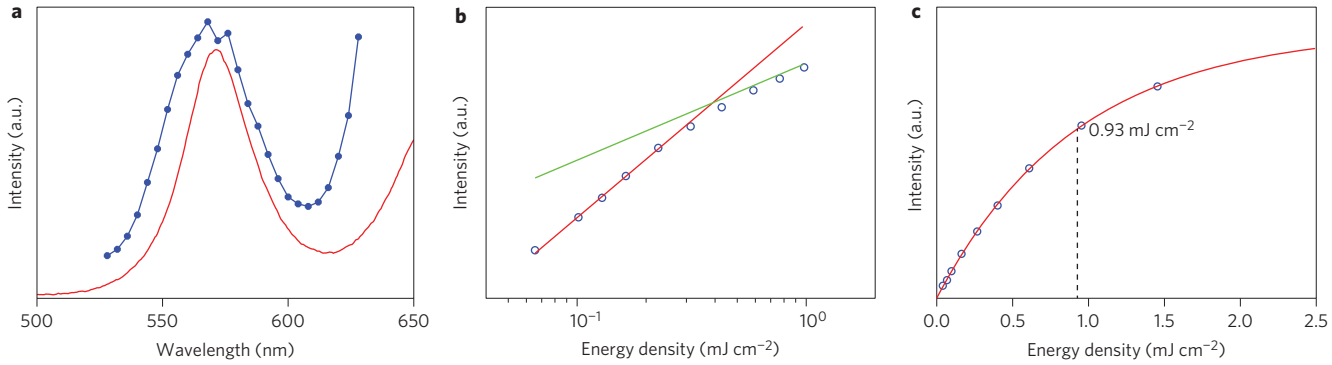

Figure 2 | Ensemble upconversion measurements. a, Emission spectrum of upconverted luminescence excited at 680 nm (blue) closely resembles the ensemble emission spectrum excited at 405 nm (red). **b**, Excitation energy density dependence of the upconverted luminescence (blue circles) together with quadratic (red) and linear (green) fits to the respective parts of the curve. **c**, Saturation of the red emission with increasing excitation pulse energy.

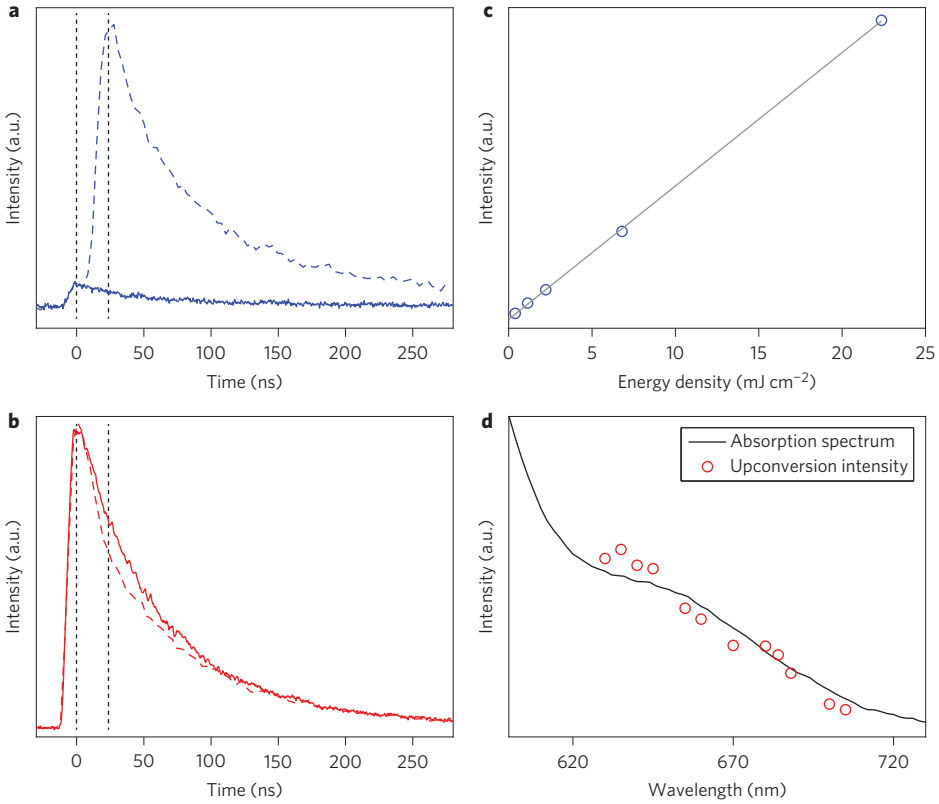

Figure 3 | Pump–probe luminescence upconversion experiments. a, The 570 nm emission transient induced by a weak 680 nm pump (continuous line) and when the pump pulse is followed by a strong 1,064 nm probe pulse (dashed line). **b**, Red emission transient with (dashed line) and without (continuous line) a delayed 1,064 nm pulse. **c**, Dependence of upconverted luminescence intensity on probe pulse energy. **d**, Upconversion luminescence intensity at fixed 1,064 nm pulse energy as a function of the wavelength of the visible pump (red circles), compared with the ensemble absorption cross-section (black line).

absorption is significantly weaker than intraband hole absorption, leaving only intraband electron absorption, which is probably of similar magnitude to intraband hole absorption, as a potential loss mechanism. The above estimate is thus correct within a factor of order unity. Because the energy density of $\sim$1 mJ cm^{-2} needs to be delivered within the lifetime of the core exciton, which is $\sim$100 ns (and is much longer than the 5 ns pulses used here), the excitation power density required for achieving this efficiency is $\sim 1 \times 10^4$ W cm^{-2}.

Finally, we performed single particle upconversion experiments. To confirm two-colour fluorescence, single quantum dot spectra were collected upon excitation with a 470 nm diode laser, as shown in Fig. 4a. A set of frames recording the emission spectral dynamics (including blinking) of the two colours at 2.5 fps (frames per second) is provided in Supplementary Section S2. For upconversion measurements, dots were excited by 690 nm light from a femtosecond oscillator, and the upconverted luminescence was measured by time-correlated single-photon counting. The excitation intensity was modulated to record the power dependence of upconverted fluorescence as portrayed in Fig. 4b. The fluorescence intermittency typically observed for single quantum dots is clearly seen. Owing to the relatively low count rate, it is difficult to determine whether the observed distribution of emission intensities is indeed due to a continuous emission intensity distribution or due to the relatively long time bins used. A distinct quadratic dependence of the emission intensity as a function of excitation intensity

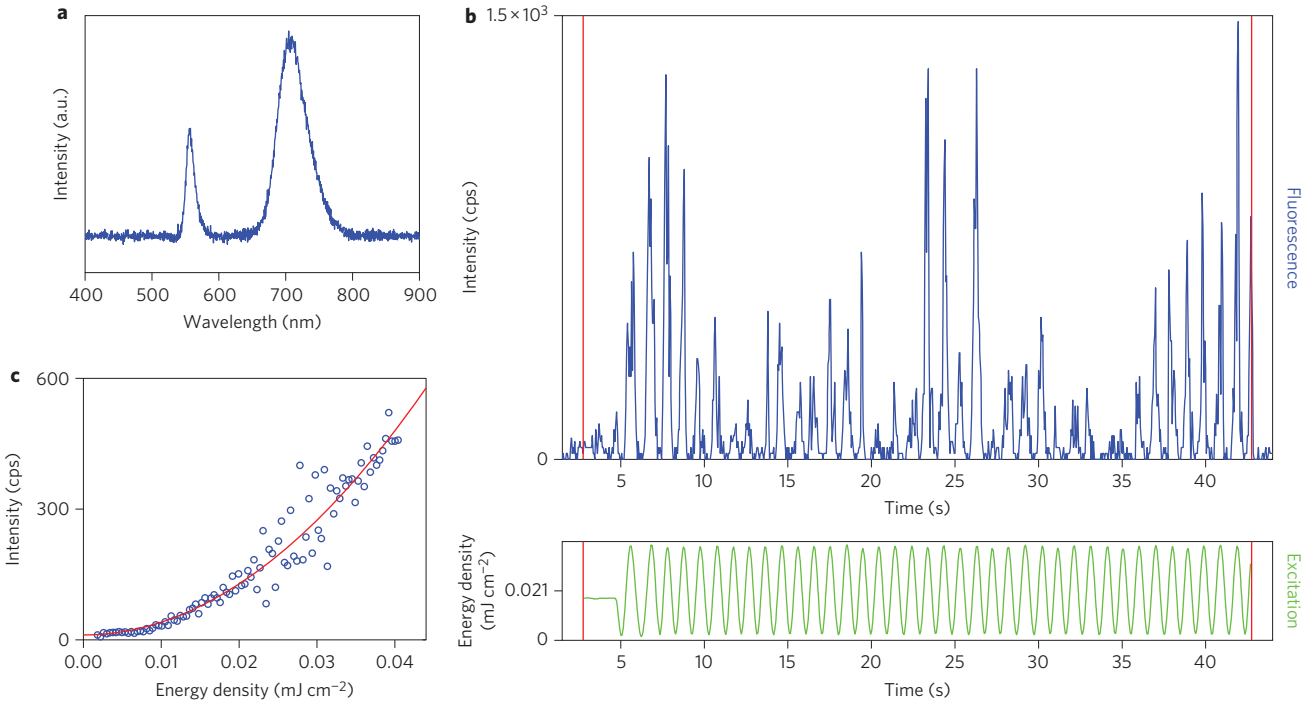

Figure 4 | Single nanocrystal upconversion measurements. a, Single dot spectrum collected over 30 s upon excitation with a 470 nm pulsed diode laser. **b**, Excitation power dependence of single-dot upconverted luminescence. Emission intensity is shown in blue in the top plot and excitation power in green in the bottom plot. Red lines show when the excitation laser was turned on and off. **c**, Binned and averaged upconverted emission intensity of a single nanocrystal as a function of excitation power (blue dots) together with a quadratic fit (red line).

is shown in Fig. 4c, and was observed for ~30 sampled particles. Typical particles exhibited upconverted luminescence of up to thousands of counts per second (cps). It should be noted that ~50% of the red-emitting quantum dots also exhibited emission around 570 nm. The vast majority of the two-colour emitting quantum dots tested exhibited upconversion.

In summary, we have devised and demonstrated a new scheme for luminescence upconversion. It is based on a colloidal solid-state configuration for which fabrication is well within the capabilities of current synthetic protocols. Because this structure is based on semiconductor components in the strongly confined regime, it provides broad tunability of both the absorption edge and the luminescence colour via size tuning. This is in stark contrast to rare-earth-doped nanocrystals, where the absorption spectra cannot easily be tuned, and where the use of 'antennas' is required to broaden the frequency response[9]. The observed 0.1% upconversion efficiency is comparable to that obtained from rare-earth-doped nanocrystals, where typical efficiencies are ~0.3% (ref. 28) and reported record efficiencies are ~1% (for particular excitation wavelengths, either 980 nm (ref. 8) or 1,490 nm (ref. 29)). The required excitation power density at saturation in our system, 1×10^4 W cm^{-2}, is two orders of magnitude higher than that observed in rare-earth-doped nanocrystals[8,9,28,29], but many orders of magnitude lower than those required for upconversion via two-photon absorption (typically ~1 GW cm^{-2}; see, for example, ref. 30 and references therein). Clear paths towards improvements in performance for the current system can be identified. One is to increase the lifetime of the low-energy state, leading to reduction of the saturation excitation density. Indeed, the use of a doped quantum dot as described here already leads to a roughly fourfold increase in lifetime relative to an undoped CdSe quantum dot, but the use of IV–VI quantum dots or indirect-gap materials could significantly increase it further. Engineering the barrier height by composition tuning is also a viable pathway towards enhanced efficiency, as is delicate tuning of the barrier length. Improved synthetic protocols can enhance the emission quantum yield of the higher energy transition, again resulting in efficiency enhancement.

The ease of manufacture of these nanocrystals and their suitability for solution processing, as well as the demonstrated compatibility of quantum dots with a variety of bioimaging applications, suggest significant promise for numerous applications. These include multiphoton microscopy with continuous-wave excitation sources, high-energy photon sources placed inside tissue (with potentially intriguing applications such as photodynamic therapy) and photovoltaics.

Methods

Nanoparticle synthesis. Tellurium-doped CdSe core nanocrystals were prepared using a procedure modified from a previous report[24]. For further seeded growth of CdS, a slight modification of previously reported methods was used[25]. The core–rod nanocrystals were separated for further growth of the CdSe dot at the tip end by multiple purification steps in known solvent/antisolvent combinations such as chloroform/methanol and toluene/acetone. They were then redissolved in a mixture of trioctyl phosphine (TOP), trioctyl phosphine oxide and oleylamine, and the solution was heated to 200 °C. Following this, small amounts of a selenium solution in TOP and of cadmium acetate in TOP were added until a second emission peak emerged at 540–550 nm. Further additions of sulphur solution in TOP and cadmium acetate in TOP over the course of 90 min led to the desired emission at 570 nm. Further synthesis details can be found in Supplementary Section S1.

Ensemble optical measurements. Samples consisted of a dilute solution of nanocrystals in toluene, placed in a 1 cm × 1 cm glass cuvette. Excitation light from a nanosecond optical parametric oscillator (Ekspla NT-UV342) was directed towards the cuvette, and fluorescence was collected in the orthogonal direction, spectrally filtered, directed towards a monochromator (Acton SP2150) and measured by a photomultiplier (Hamamatsu R11540). The photomultiplier transient output was measured by a digital oscilloscope (LeCroy Wavesurfer 62Xs). For pump–probe measurements, the residual 1,064 nm pump laser was passed through an optical delay line and recombined with the excitation beam using a dichroic mirror.

Sample preparation for single quantum dot spectroscopy. A 2% (wt/vol) solution of polymethylmethacrylate (PMMA) in toluene was prepared for incorporation of

the nanocrystals in a thin film. A mild extraction of the nanocrystals from the mother solution was carried out by dissolving a small amount in hexane/octadecene and adding acetone/methanol for phase separation. The nanocrystal phase was then diluted in hexane, filtered, and then diluted again tenfold in toluene to give an almost colourless solution. A volume of 100 μl of this solution was diluted in 1 ml PMMA/toluene. This solution was then spincast onto glass slides at a speed of 8,000 r.p.m. The resulting intra-quantum dot spacing was ~15 μm.

Single nanoparticle imaging and spectroscopy. Single-dot optical measurements were performed using a custom-built optical characterization system based on a commercial inverted microscope (Zeiss Axiovert 200). Imaging of the film was achieved with 475 nm light-emitting diode wide-field illumination in a transmission set-up. Photoluminescence was imaged through an oil immersed objective (Zeiss Plan Apochromat ×63, NA 1.4) and two spectrally exclusive bandpass filters for recognizing the two emission colours (540–580 nm and 690–740 nm) onto an electron-multiplying charge-coupled device (CCD) camera (Acton-PI PhotonMax 512). For illumination of a single nanocrystal we used a 690 nm Ti:sapphire laser emitting 100 fs pulses at a repetition rate of 80 MHz. The signal was epi-collected, coupled to a multimode fibre, and measured by an avalanche photodiode (Laser Components count blue or Perkin Elmer SPDC). The avalanche photodiode signal was evaluated by a time-correlated single-photon counting device (Picoquant Hydraharp 400) triggered by the excitation laser. For measurement of the upconversion signal a 590 nm short-pass dichroic mirror was used.

The power of the incoming beam was modulated by passing it through a rotating waveplate and a polarizer. Part of the beam was diverted to a photodiode for power measurement (Ophir PD300-UV and Juno power meter), allowing continuous monitoring of the power throughout the measurement.

Excitation of individual nanocrystals for spectroscopic measurements was carried out with a tightly focused beam of a 473 nm pulsed diode laser emitting 70 ps pulses at a 5 MHz repetition rate (Edinburgh Instruments EPL 470). The energy flux was ~2.4 μJ cm^{-2} per pulse. Emitted photons were imaged onto a fibre bundle coupling the light to a spectrometer (Acton-PI SP2300), equipped with a four-stage thermoelectrically cooled CCD camera (Acton-PI Pixis 256).

Received 17 January 2013; accepted 25 June 2013; published online 4 August 2013

References

1. Wang, F., Banerjee, D., Liu, Y., Chen, X. & Liu, X. Upconversion nanoparticles in biological labeling, imaging, and therapy. *Analyst* **135,** 1839–1854 (2010).
2. Zhou, J., Liu, Z. & Li, F. Upconversion nanophosphors for small-animal imaging. *Chem. Soc. Rev.* **41,** 1323–1349 (2012).
3. De Wild, J., Meijerink, A., Rath, J. K., Van Sark, W. G. J. H. M. & Schropp, R. E. I. Upconverter solar cells: materials and applications. *Energy Environ. Sci.* **4,** 4835–4848 (2011).
4. Menyuk, N. $NaYF_4$: Yb,Er—an efficient upconversion phosphor. *Appl. Phys. Lett.* **21,** 159–161 (1972).
5. Haase, M. & Schäfer, H. Upconverting nanoparticles. *Angew. Chem. Int. Ed.* **50,** 5808–5829 (2011).
6. Shockley, W. & Queisser, H. J. Detailed balance limit of efficiency of p–n junction solar cells. *J. Appl. Phys.* **32,** 510–519 (1961).
7. Wu, S. *et al.* Non-blinking and photostable upconverted luminescence from single lanthanide-doped nanocrystals. *Proc. Natl Acad. Sci. USA* **106,** 10917–10921 (2009).
8. Chan, E. M. *et al.* Combinatorial discovery of lanthanide-doped nanocrystals with spectrally pure upconverted emission. *Nano Lett.* **12,** 3839–3845 (2012).
9. Zou, W., Visser, C., Maduro, J. A., Pshenichnikov, M. S. & Hummelen, J. C. Broadband dye-sensitized upconversion of near-infrared light. *Nature Photon.* **6,** 560–564 (2012).
10. Parker, C. A. & Hatchard, C. G. Sensitised anti-Stokes delayed fluorescence. *Proc. Chem. Soc.* 386–387 (1962).
11. Baluschev, S. *et al.* Up-conversion fluorescence: noncoherent excitation by sunlight. *Phys. Rev. Lett.* **97,** 7–9 (2006).
12. Cheng, Y. Y. *et al.* Improving the light-harvesting of amorphous silicon solar cells with photochemical upconversion. *Energy Environ. Sci.* **5,** 6953–6959 (2012).
13. Singh-Rachford, T. N. & Castellano, F. N. Photon upconversion based on sensitized triplet–triplet annihilation. *Coord. Chem. Rev.* **254,** 2560–2573 (2010).
14. Mokari, T., Rothenberg, E., Popov, I., Costi, R. & Banin, U. Selective growth of metal tips onto semiconductor quantum rods and tetrapods. *Science* **304,** 1787–1790 (2004).
15. Amirav, L. & Alivisatos, A. P. Photocatalytic hydrogen production with tunable nanorod heterostructures. *J. Phys. Chem. Lett.* **1,** 1051–1054 (2010).
16. Anshu, P. & Guyot-Sionnest, P. Slow electron cooling in colloidal quantum dots. *Science* **322,** 929–932 (2008).
17. Deutsch, Z., Schwartz, O., Tenne, R., Popovitz-Biro, R. & Oron, D. Two-color antibunching from band-gap engineered colloidal semiconductor nanocrystals. *Nano Lett.* **12,** 2948–2952 (2012).
18. Klimov, V. I., Mikhailovsky, A. A., McBranch, D. W., Leatherdale, C. A. & Bawendi, M. G. Quantization of multiparticle auger rates in semiconductor quantum dots. *Science* **287,** 1011–1013 (2000).
19. Yang, Y., Zhang, Y. H., Shen, W. Z. & Liu, H. C. Semiconductor infrared up-conversion devices. *Prog. Quantum Electron.* **35,** 77–108 (2011).
20. Heimbrodt, W., Happ, M. & Henneberger, F. Giant anti-Stokes photoluminescence from semimagnetic heterostructures. *Phys. Rev. B* **60,** R16326–R16329 (1999).
21. Potemski, M. *et al.* Auger recombination within Landau levels in a two-dimensional electron gas. *Phys. Rev. Lett.* **66,** 2239–2242 (1991).
22. Seidel, W., Titkov, A., André, J., Voisin, P. & Voos, M. High-efficiency energy up-conversion by an 'Auger fountain' at an InP–AlInAs type-II heterojunction. *Phys. Rev. Lett.* **73,** 2356–2359 (1994).
23. Cheong, H., Fluegel, B., Hanna, M. & Mascarenhas, A. Photoluminescence up-conversion in $Al_xGa_{1-x}As$ heterostructures. *Phys. Rev. B* **58,** 4254–4257 (1998).
24. Avidan, A. & Oron, D. Large blue shift of the biexciton state in tellurium doped CdSe colloidal quantum dots. *Nano Lett.* **8,** 2384–2387 (2008).
25. Carbone, L. *et al.* Synthesis and micrometer-scale assembly of colloidal CdSe/CdS nanorods prepared by a seeded growth approach. *Nano Lett.* **7,** 2942–2950 (2007).
26. Talapin, D. V *et al.* Seeded growth of highly luminescent CdSe/CdS nanoheterostructures with rod and tetrapod morphologies. *Nano Lett.* **7,** 2951–2959 (2007).
27. Woggon, U., Winda, O., Langbeina, W., Gogolinb, O. & Klingshirna, C. Confined biexcitons in CuBr quantum dots. *J. Lumin.* **59,** 135–145 (1994).
28. Boyer, J-C. & van Veggel, F. C. J. M. Absolute quantum yield measurements of colloidal $NaYF_4:Er^{3+},Yb^{3+}$ upconverting nanoparticles. *Nanoscale* **2,** 1417–1419 (2010).
29. Chen, G., Ohulchanskyy, T. Y., Kachynski, A., Agren, H., Prasad, P. N. Intense visible and near-infrared upconversion photoluminescence in colloidal $LiYF_4:Er^{3+}$ nanocrystals under excitation at 1490 nm. *ACS Nano* **5,** 4981–4986 (2011).
30. Xing, G. *et al.* Ultralow-threshold two-photon pumped amplified spontaneous emission and lasing from seeded CdSe/CdS nanorod heterostructures. *ACS Nano* **6,** 10835–10844 (2012).

Acknowledgements

The authors acknowledge financial support from the Minerva Foundation, the Leona M. and Harry B. Helmsley charitable trust, and the European Research Council (starting investigator grant SINSLIM 258221). D.O. is the incumbent of the Recanati Career Development Chair in Energy Research.

Author contributions

Z.D. synthesized the nanocrystals. L.N. and Z.D. performed the optical experiments. D.O. conceived and supervised the project. The manuscript was written jointly by all authors.

Additional information

Supplementary information is available in the online version of the paper. Reprints and permissions information is available online at www.nature.com/reprints. Correspondence and requests for materials should be addressed to D.O.

Competing financial interests

The authors declare no competing financial interests.